Original Research

Characterizing Iron Deposition in Multiple Sclerosis Lesions Using Susceptibility Weighted Imaging

E. Mark Haacke, PhD,[1,2,3,*] Malek Makki, PhD,[1] Yulin Ge, MD,[4] Megha Maheshwari, MS,[2] Vivek Sehgal, MD,[1] Jiani Hu, PhD,[1] Madeswaran Selvan, MS,[2] Zhen Wu, MD,[3] Zahid Latif, RT,[1] Yang Xuan, PhD,[1] Omar Khan, MD,[5] James Garbern, MD, PhD,[5] and Robert I. Grossman, MD[4]

Purpose: To investigate whether the variable forms of putative iron deposition seen with susceptibility weighted imaging (SWI) will lead to a set of multiple sclerosis (MS) lesion characteristics different than that seen in conventional MR imaging.

Materials and Methods: Twenty-seven clinically definite MS patients underwent brain scans using magnetic resonance imaging including: pre- and postcontrast T1-weighted imaging, T2-weighted imaging, FLAIR, and SWI at 1.5 T, 3 T, and 4 T. MS lesions were identified separately in each imaging sequence. Lesions identified in SWI were re-evaluated for their iron content using the SWI filtered phase images.

Results: There were a variety of new lesion characteristics identified by SWI, and these were classified into six types. A total of 75 lesions were seen only with conventional imaging, 143 only with SWI, and 204 by both. From the iron quantification measurements, a moderate linear correlation between signal intensity and iron content (phase) was established.

Conclusion: The amount of iron deposition in the brain may serve as a surrogate biomarker for different MS lesion characteristics. SWI showed many lesions missed by conventional methods and six different lesion characteristics. SWI was particularly effective at recognizing the presence of iron in MS lesions and in the basal ganglia and pulvinar thalamus.

Key Words: multiple sclerosis; iron deposition; susceptibility weighted imaging; phase imaging
J. Magn. Reson. Imaging 2009;29:537–544.

MULTIPLE SCLEROSIS (MS) is an inflammatory demyelinating and neurodegenerative disease of the central nervous system (1,2). Most patients start with a relapsing-remitting course, which has a clearly defined episode of neurologic disability and recovery. The pathologic hallmark of multiple sclerosis is the demyelinated plaque, a well-demarcated hypocellular area characterized by the loss of myelin, along with axonal loss due to (3,4), and the formation of astrocytic scars. The etiologic mechanism underlying MS is generally believed to be autoimmune inflammation (5). Nevertheless, what initiates the disease and the sequence of events underlying the development of MS is not yet well established (6).

Conventional magnetic resonance imaging (MRI) has been used routinely to diagnose and monitor the disease spatially and temporally. The use of conventional MRI to measure disease activity and assess effects of therapy is now standard in clinical practice and drug trials (7). T2-weighted imaging (T2WI) is highly sensitive in the detection of hyperintensities in white matter. However, hyperintensities on T2WI can correspond to a wide spectrum of pathology, ranging from edema and mild demyelination to lesions in which the neurons and supporting glial cells are replaced by glial scars or liquid necrosis (8–14). In addition to T2WI, Gadolinium enhancement on T1-weighted imaging (T1WI) can suggest acute inflammation, which is a marker of disease

[1]Department of Radiology, Wayne State University, Detroit, Michigan, USA.
[2]Department of Biomedical Engineering, Wayne State University, Detroit, Michigan, USA.
[3]Department of Biomedical Engineering, McMaster University, Hamilton, Ontario, Canada.
[4]Department of Radiology, New York University, New York, New York, USA.
[5]Department of Neurology, Wayne State University, Detroit, Michigan, USA.

Contract grant sponsor: the National Institutes of Health. Contract grant number: R01NS029029. Contract grant sponsor: the State of Michigan. Contract grant number: 085P5200251. Contract grant sponsor: the Multiple Sclerosis Society. Contract grant number: CA1042-A-8.

*Address reprint requests to: E.M.H., MR Research Facility, Department of Radiology, Wayne State University, HUH—MR Research G030/Radiology, 3990 John R Road, Detroit, MI 48201. E-mail: nmrimaging@aol.com

Received June 10, 2008; Accepted November 3, 2008
DOI 10.1002/jmri.21676
Published online in Wiley InterScience (www.interscience.wiley.com).

Table 1
Imaging Parameters for Conventional Sequences at 1.5 T

	1.5 T							
	No. of Slices	Slice Thickness (mm)	FOV (mm)	TR (ms)	TE (ms)	BW (Hz/pixel)	FA	Resol. (mm)
T1-pre	45	3	256	630	15	110	90°	1 × 1 × 3
T2	45	3	256	2800	16	100	180°	1 × 1 × 3
FLAIR	45	3	240	8800	125	130	180°	1 × 1 × 3
T1-post	45	3	256	630	15	110	90°	1 × 1 × 3

activity (15). Newer MRI techniques, including magnetization transfer ratio (MTR) imaging, magnetic resonance spectroscopy (MRS), diffusion tensor imaging (DTI), and quantitative analysis of changes in brain volume (brain atrophy) are applied in MS to detect diffuse damage of axons and neurons. These MRI techniques have limited and different specificities toward various elements of MS pathology (16–19).

It is becoming a consensus among many studies that iron is enriched within oligodendrocytes and myelin in both normal and diseased tissue (20–23). One explanation for such findings proposes that iron is associated with the biosynthetic enzymes of myelinogenesis (24). In the case of demyelinating diseases, the mechanism of damage to the brain by iron might be related to oxidative stress induced by the generation of toxic-free radicals (20). Brain iron accumulation has been shown histologically in neurodegenerative diseases, including MS (25,26), and has been specifically seen in the vessel walls of veins (27). Recently, more studies have been investigating hypointensities on T2WI, which suggest iron deposition in the dentate nucleus, the cortex and adjacent subcortical white matter, the brain stem, the basal ganglia, and the thalamus. The results of these studies have suggested that hypointensities in T2WI were highly related to brain atrophy, disease course, and physical disability (28–30). However, such studies were based on conventional or fast spin-echo T2WI, which is not sufficient for detecting a subtle iron component that may be associated with lesion development and progression. A fairly new technique, magnetic field correlation imaging (31), has been used to quantitatively assess iron accumulation in the deep gray matter. This is a low-resolution technique that attempts to measure local magnetic field inhomogeneities to assess iron accumulation. Susceptibility weighted imaging (SWI) has been shown to be very sensitive to iron in the form of hemosiderin, ferritin, and deoxyhemoglobin (32,33), offering the ability to measure iron on the order of several μg/g of tissue in vivo (34). SWI is a 3D, high-resolution, fully flow-compensated gradient-echo sequence that uses magnitude and phase data both separately and together to enhance information about local tissue susceptibility.

In the past, phase images were seldom used because artifacts from the background field destroyed the integrity of small changes seen in pristine tissue. As we know now, phase images contain a wealth of information that may not be observed from the magnitude image. Recently, SWI-filtered phase images were used to map out putative iron content in the brain (35). Phase images are a direct measure of the sources of local susceptibility changes (34,36,37). In this study, we explore the new contrast and information provided by SWI as it applies to imaging multiple sclerosis lesions. Given the perivascular (venous) relationship with MS, specifically the fact that there is vessel wall breakdown in the veins (27), we hypothesize that signal measured on SWI phase will provide a unique signature for iron accumulation. The goal of this study is to investigate whether the variable forms of putative iron deposition seen in SWI will lead to a set of lesion characteristics different than that seen in conventional MR imaging.

MATERIALS AND METHODS

Twenty-seven clinically definite MS patients (21 females and 6 males, aged from 21 to 71 years old with a mean age of 45 years; all patients signed an institutional review board [IRB]-approved consent form) (38) underwent clinical brain MRI scans including: 3D T1-weighted MPRAGE, axial T2W, FLAIR, and contrast-enhanced T1W imaging at 1.5 T, 3 T, and 4 T. (The 3 T data sets did not have FLAIR images.) Detailed parameters for these sequences are provided in Tables 1–3. In addition to these conventional MRI sequences, patients underwent 3D SWI to acquire simultaneously phase and magnitude images. A special high-pass (homodyne) filter was used to remove most of the low spatial frequency background field artifacts (4,19,39). Usually, a 64 × 64 low spatial frequency kernel is used to com-

Table 2
Imaging Parameters for Conventional Sequences at 3T

	3 T*							
	# of Slices	Slice Thickness (mm)	FOV (mm)	TR (ms)	TE (ms)	BW (Hz/pixel)	FA	Resol. (mm)
T1-pre	50	3	220	500	7	220	90°	0.5 × 0.5 × 3
T2	96	3	256	5000	101	200	121°	1 × 1 × 3
T1-post	50	3	220	500	7	220	90°	0.5 × 0.5 × 3

*FLAIR scans were not performed.

Table 3
Imaging Parameters for Conventional Sequences at 4T

	4 T							
	No. of Slices	Slice Thickness (mm)	FOV (mm)	TR (ms)	TE (ms)	BW (Hz/pixel)	FA	Resol. (mm)
T1-pre	32	2	256	28	15	80	12°	1 × 1 × 2
T2	29	4	256	4000	72	120	150°	0.8 × 0.8 ×
FLAIR	24	4	256	6870	116	200	150°	0.5 × 0.5 ×
T1-post	32	2	256	28	15	80	12°	1 × 1 × 2

plex-divide into the original data to create an effective high-ass filtered phase image. The resulting image is referred to as the "SWI filtered phase image."

1.5 T

Fourteen patients (aged 21 to 68 years old, with a mean age of 44 years) were scanned on a 1.5 T Sonata (Siemens, Erlangen, Germany). The image parameters for SWI were: a slab of 64 slices with a 2-mm thickness, no gap, a field of view (FOV) of 256 mm, an acquisition matrix of 512 × 256, a pulse repetition time (TR)/echo time (TE) of 85/35 msec and a flip angle of 25°. This was a turbo-SWI segmented echo-planar-like sequence with five echoes and phase encoding between echoes to save time. The total scan time for all sequences was about 45 min.

3.0 T

Seven patients (aged 41 to 67 years old, with a mean age of 50 years old) were scanned on a 3.0 T Trio (Siemens). The image parameters for SWI were: a slab of 64 slices with a 2-mm thickness, no gap, an FOV of 220 mm, an acquisition matrix of 512 × 512, a TR/TE of 50/25 msec, and a flip angle of 20°. This was a conventional (single-echo) gradient-echo acquisition. The total scan time for all sequences was about 45 min.

4.0 T

Six patients (aged 21 to 71 years old, with a mean age of 42 years old) were scanned on a 4 T magnet (Brucker/Siemens). The image parameters for SWI were: a slab of 64 slices with a 2-mm thickness, no gap, an FOV of 256 mm, an acquisition matrix of 512 × 256, a TR/TE of 24/15 msec, and a flip angle of 12°. This was a conventional single echo acquisition. The total scan time for all sequences was about 40 min.

Lesion Identification

MS lesions on conventional MRI sequences were identified by an experienced neuroradiologist. Lesions on SWI phase images were identified by consensus between three experienced MR researchers after consultation with the neuroradiologist. SWI was compared with conventional T2W, T1W, and FLAIR (except at 3 T). Lesions seen on SWI were hand drawn, overlaid onto conventional T2W and FLAIR images, and their shapes and patterns were compared.

Iron Quantification

Phase is determined by the following function (for a left-handed system):

$$\phi = \gamma \cdot \Delta B \cdot \mathrm{TE} \quad [\mathrm{rad}] \qquad [1]$$

where γ is the gyromagnetic ratio (MHz/*T*), ΔB (*T*) is the change in magnetic field between tissues, and TE is the echo time (msec). Iron is a paramagnetic element and aligns along the main magnetic field producing a larger field, that is, ΔB is positive. At a given TE, the more iron

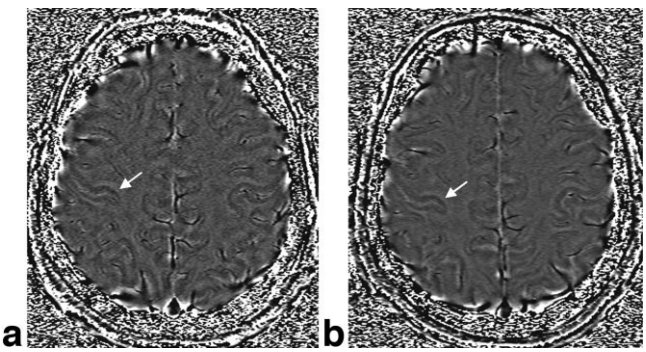

Figure 1. Phase images at 1.5T (**a**) and 3T (**b**) of the same patient with B_0TE kept constant. The central sulcus (arrow) is clearly seen in both individuals. The gray/white matter contrast in these images comes from the increased MR visible iron content in the gray matter giving it an appearance similar to a T1-weighted scan.

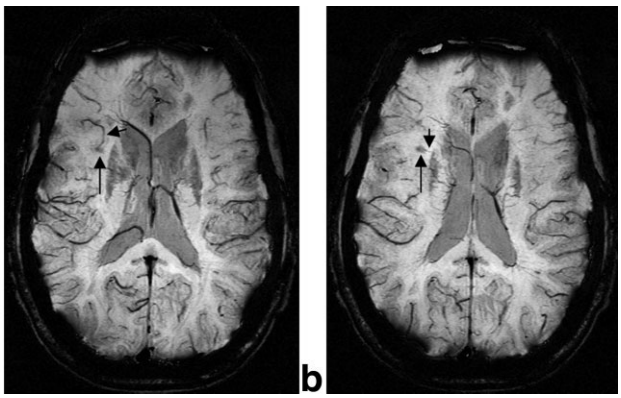

Figure 2. Two SWI processed images of adjacent slices acquired at 3 T. Note the connectivity between the iron-containing lesion (the dark nodule, long arrow) and a peripheral vein that curls up toward the lateral right side of the brain (**a**, short arrow) and a vein that connects to the putamen (**b**, short arrow).

Table 4
Counts and Categories of Lesions Seen on SWI

Category	Description	1.5 T	3 T	4 T
A	Uniform darkening of lesions in phase	101 (63 m)	46 (38 m)	72 (33 m)
B	Magnitude lesions not seen with phase	7	32	31
C	Lesions associated with veins	6	3	4
D	Lesions surrounded by a rim of hypointense signal	7	1	3
E	Lesions with central darkening of signal	4	1	1
F	Gray matter lesions (including the basal ganglia)	16	6 (1 m)	5
Total		141	90	116

m = magnitude.

content in the tissue, the more the phase differs from zero. Therefore, the contrast seen in a brain image, for example, will depend on how much iron is present. This can be expressed as follows:

$$\Delta B = \Delta\chi B_0 \quad [2]$$

$$\Delta\chi \propto c$$

where c is the concentration of iron and $\Delta\chi$ is the change in susceptibility (in ppm). Thus, any changes in the amount of iron will lead to changes in the phase of the tissue relative to its surroundings. From [1] and [2], it is evident that phase will remain invariant if the product of B_0 and TE remains constant.

Siemens uses the following phase convention:

$$\Phi = 2048\,[(\phi/\pi) + 1]$$

In addition to showing that 3 Siemens phase units (Φ) correspond to 1 μg Fe/g tissue, a recent study has established a baseline of phase differences between tissues in a number of brain regions for normal people (35). To evaluate the iron content in MS patients, regions of interest (ROIs) were chosen in three separate areas: lesions, the area immediately surrounding lesions, and normal-appearing white and gray matter (using T2W and FLAIR images to distinguish between white and gray matter). The area immediately surrounding lesions was defined by carefully tracing lesion boundaries seen in each slice. Around this was drawn another larger boundary—creating effectively an annular boundary region. Combining this evaluation with a comparison of lesions' appearance on conventional images allowed the areas inside and outside of lesion boundaries to be well characterized. The average phase value of each ROI was measured using the in-house software, SPIN (Signal Processing in NMR). The iron content on SWI phase images was then correlated with the signal intensity of the same ROI measured on T2W images using a simple linear regression.

Of the 27 patient data sets processed, one had widespread lesions covering the entire white matter structures and was not analyzed for the purpose of this investigation. Another patient did not show any lesions in any clinical MRI sequence, as well as SWI, and was thus excluded from our study.

RESULTS

Phase data were compared between 1.5 T, 3 T, and 4 T. The imaging parameters for SWI were designed so that the product of B_o and TE remained constant. An example phase image from the same volunteer at 1.5 T and 3 T (Fig. 1) shows that the phase is invariant as expected. For example, the phase in the motor cortex was measured to be 2155 $\pm$ 31 phase units for 1.5 T and 2120 $\pm$ 17 phase units for 3 T. After reviewing the data, it was evident that there were lesions clearly seen with SWI but not with FLAIR or T2WI, and also those seen with FLAIR or T2WI but not with SWI. There was a variety of lesion characteristics seen in the SWI phase images (see Table 4) and we were able to categorize them according to the following six properties: (a) uniform darkening of

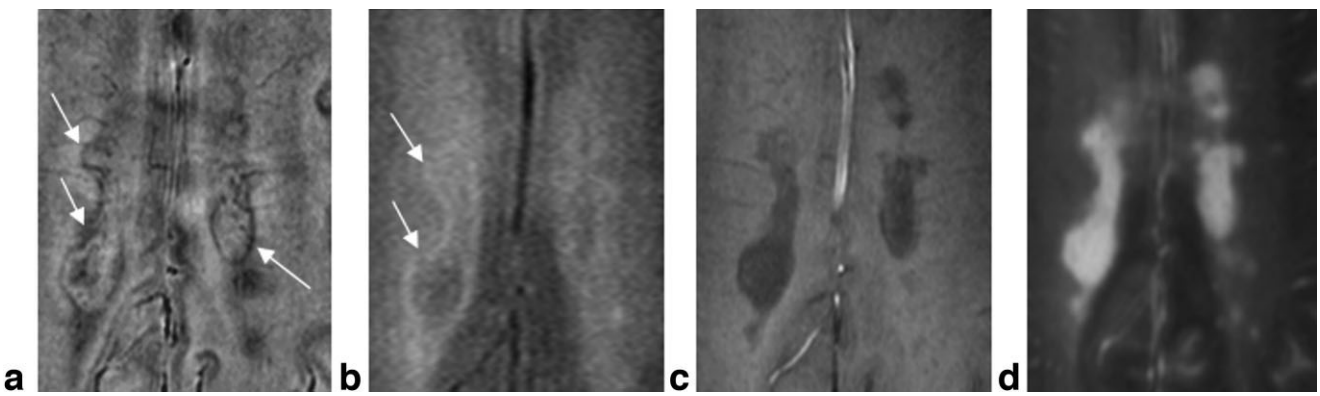

Figure 3. The rims of lesions (arrows) are seen more clearly in SWI phase (**a**) than in FLAIR (**b**). The rims are not defined in magnitude (**c**) or T2 (**d**). This data was acquired at 4 T.

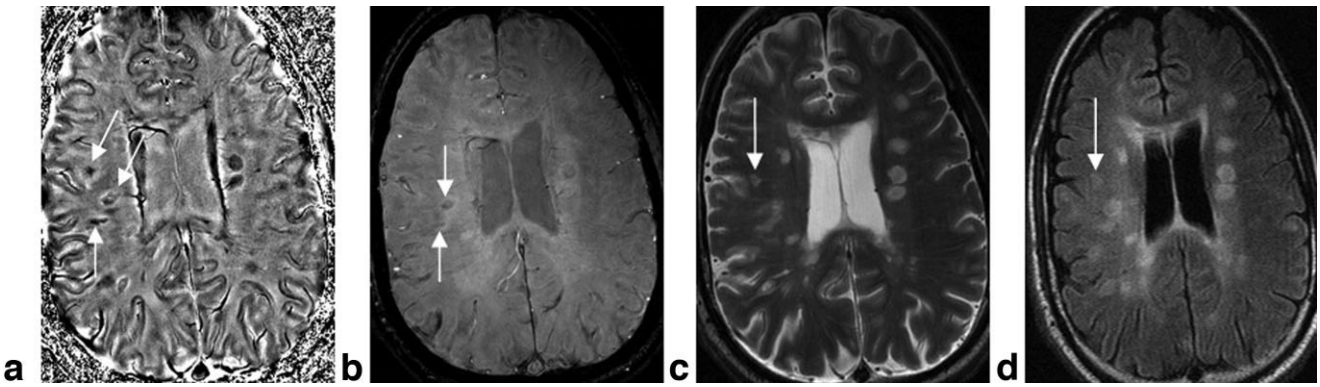

Figure 4. Lesions with high phase/iron content, as shown in SWI filtered phase images (**a**) are either not visible or less clearly seen in SWI magnitude (**b**), T2-weighted (**c**) or FLAIR images (**d**) at 4T.

lesions in phase images; (b) lesions seen in the magnitude SWI data but not in the phase; (c) lesions associated with veins; (d) lesions surrounded by a rim of hypointense signal; (e) lesions with a central darkening of signal; and (f) gray matter lesions (including one in the basal ganglia). Some representative examples of these lesions and their comparisons with conventional imaging are shown in Figures 2 through 6.

A total of 422 lesions were identified by all methods; 75 were not seen with SWI, and 143 were not seen with conventional methods but were detected by SWI. A total of 204 lesions were seen with both methods. A detailed summary of all lesions measured for each field strength appears in Tables 5, 6, and 7. In each table, the number in parentheses followed by an "m" represents how many of the phase lesions were also seen in the magnitude data.

Iron Quantification Using SWI Phase Images

A total of 199 uniform phase lesions were evaluated from eight patients who had enough lesions to draw a correlation. These patients were imaged at various field strengths. The average phase value in the lesions was 2186 ± 42 while the surrounding normal-appearing white matter had an average phase value of 2044 ± 20. The difference between these two values is 142 units, representing an average iron content of 47 μg Fe/g tissue (34). (In most of the cases, the region adjacent to the lesion had iron concentrations slightly lower than those in the white matter.) A histogram of the iron content in 177 of the most well-defined lesions from the 26 analyzed patients (measured at 1.5 T, 3 T, and 4 T) is shown in Figure 7.

The signal intensity changes in lesions seen with both SWI and T2 relative to the surrounding normal-appearing white matter were seen to be moderately linearly correlated. Specifically, the SWI filtered phase was compared to the signal intensity in T2W images. The correlations between T2 signal intensity and phase/iron are summarized in Table 8 and two example plots are shown in Figures 8 and 9.

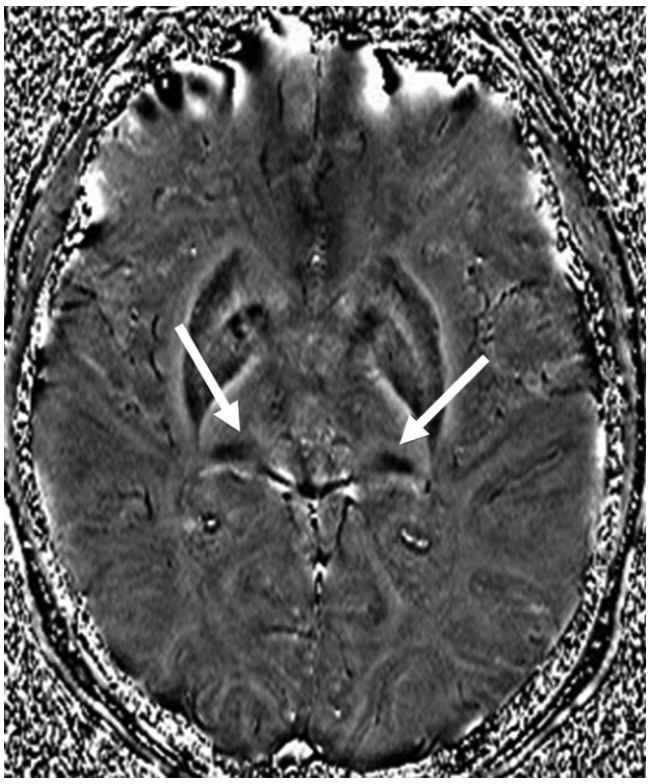

Figure 5. Filtered phase SWI image acquired at 3 T showing high iron deposition (white arrows) in the left and right pulvinar thalamus.

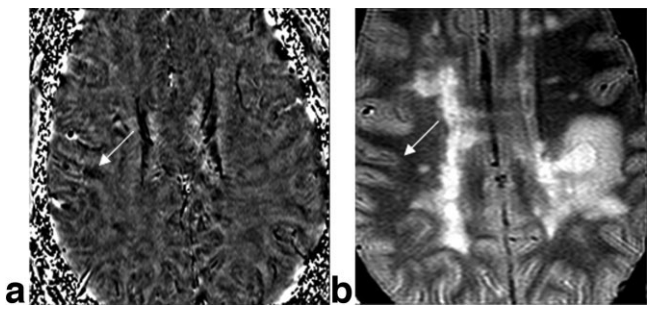

Figure 6. Possible gray matter lesions seen in an SWI phase image (**a**) and a T2W image (**b**) for data acquired at 1.5 T.

Table 5
Lesion Counts for 14 Patients at 1.5 T

	T2	T2-FLAIR	FLAIR	SWI Only	Total
Seen on SWI	30	30	3	78	141
Not seen on SWI	18	27	3		48
Total	48	57	6	78	189

Table 6
Lesion Counts for Seven Patients at 3 T

	T2	SWI Only	Total
Seen on SWI	38 p + 32 m	20	90
Not seen on SWI	21		21
Total	91	20	111

m = magnitude, p = phase.

Table 7
Lesion Counts for Six Patients at 4 T

	T2	FLAIR	SWI Only	Total
Seen on SWI	33 p + 18 m	20	45	116
Not seen on SWI		6		6
Total	51	26	45	122

m = magnitude, p = phase.

DISCUSSION

Susceptibility weighted imaging offers a unique way to view tissues affected by iron deposition whether in the form of deoxyhemoglobin, ferritin, or hemosiderin. Not only have we demonstrated that there are nearly 50% more lesions seen in total combining conventional imaging with SWI, but the iron content that makes lesions visible in SWI can also be quantified. The distribution of iron in the lesions in Figure 7 shows that the peak iron can reach 60 μg Fe/g tissue. This is as large as the iron content expected in the motor cortex. With the imaging parameters used here, recent results suggest that at 1.5 T in an ROI of 100 pixels, it is possible to determine changes in iron of just 1 μg Fe/g tissue (35). This may serve as a means to monitor iron changes over time in the lesions.

Of the six different types of lesions observed, most seem to have a fairly uniform distribution of iron. In 13 cases, we can see the direct connectivity of lesions with veins. In six others, only the center of the lesion is dark. There were, however, lesions that exhibited a ring-like structure of high iron content (11 lesions). This may be similar to the ring-like effects seen both pathologically

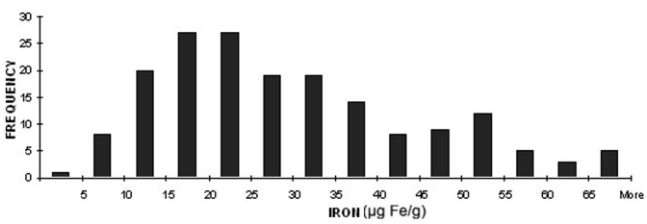

Figure 7. Histogram showing the distribution of iron deposition in well-defined lesions of the 26 analyzed patients. (These concentrations were calculated assuming that 180 Siemens phase units correspond to 60 μg Fe/g tissue.)

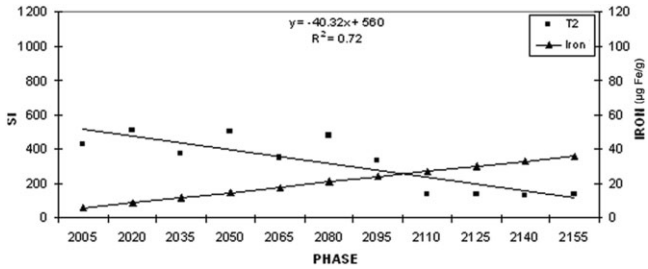

Figure 8. A plot of signal intensity from T2 versus phase and a plot of phase converted into iron content.

in leukoencephalopathy and also sometimes visible on FLAIR and T2WI. The ability to see these rims of iron (Fig. 3) may also have an impact on disease progress (15). Finally, there is some evidence of gray matter abnormality (28 lesions).

Differentiating simple changes in phase from veins was done by looking for connectivity. Usually, it was fairly easy to discriminate between signal changes caused by veins and those corresponding to lesions because we could view the mIP of three or more slices centered on the slice of interest. These mIP images show the connectivity of the vessels and make it clear if the vessel runs through the lesion of interest. Most of the lesions, however, showed fairly large nonvascular structures that were not circular in nature. Because these lesions often sat in white matter, and because the phase of white matter is close to zero, it is fairly obvious, with practice, what represents an abnormal phase signal, and hence its probability of being a lesion. We read the phase images separately and then compared the results to the FLAIR or T2 data. Because many of the lesions do overlap with T2 lesions, this gave us good confidence that our interpretations of these new findings were likely correct. As a comparison with T1, T2, and FLAIR, we used a "copy ROI" feature in our software to ensure the appropriate interpretation and registration of the lesions. Because all sequences were run with the same FOV, this was a particularly easy way to ensure that we were looking at the same lesions. When these ROIs were copied from one image to the next, we observed that the shapes of the ring lesions seen on the SWI data were essentially identical to the shape on the corresponding T2W images.

Why is this new biomarker for iron potentially important in the study of MS with SWI? The current MR imaging biomarkers of MS pathology focus on: the

Table 8
Correlations between T2 Signal Intensity and Phase/Iron Content

Patient	r_{T2}	p_{T2}
1	−0.87	0.010
2	−0.34	0.230
3	−0.39	0.270
4	−0.59	0.020
5	−0.11	0.680
6	−0.34	0.320
7	−0.78	0.005
8	−0.83	0.022

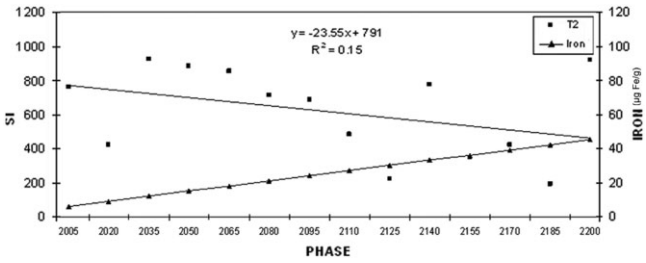

Figure 9. A plot of signal intensity from T2 versus phase and a plot of phase converted into iron content.

breakdown of the blood–brain barrier, multifocal inflammation, demyelination, oligodendrocyte loss, axonal and neuronal degeneration, gliosis, and remyelination and repair (40). In a systematic analysis of all studies published in the last 20 years, it was found that none of the proposed biomarkers could serve as a surrogate marker for clinical outcome (41). In a disease with a complex pathogenesis, such as MS, an individual biomarker is likely to reflect only one aspect of many pathogenic processes. The ability to predict the outcome of MS is complicated due to the underlying diversity and variability of the lesions. Although clinical judgment and experience provide the foundation for medical decisions, advances in neuroimaging may enhance the management of these patients if more specific biomarkers can be found.

Iron may be yet another critical means by which to assess the status of MS patients. Iron is a paramagnetic substance that reduces T2 relaxation time, resulting in hypointensity on T2-weighted images. The different types of nonheme iron in the brain include low-molecular-weight complexes, ionic iron, metalloproteins such as transferrin, melanotransferrin, and lactoferrin, as well as storage proteins such as ferritin and hemosiderin (34). Transferrin carries iron from the blood into tissues, while ferritin stores excess iron atoms that are not immediately engaged in metabolic activities. There can be up to 4500 iron atoms stored in the 8 nm-diameter internal cavity of one ferritin protein (34). Hemosiderin is considered to be a water-soluble iron storage molecule that is a breakdown product of ferritin and appears to be associated with iron overload disorders and hemorrhage (34). Brain iron accumulation has been shown histologically in MS and recently, an iron increase from 24% to 39.5% was reported in the deep gray matter in MS patients compared to control subjects (25,26).

The source of iron deposition may be myelin/oligodendrocyte debris (17), concentrated iron in the macrophages (that phagocytize the myelin/oligodendrocyte), or the product of hemorrhages from damaged brain vessels. The mechanism of direct damage to the brain by iron might be related to oxidative stress and the generation of toxic-free radicals (12). The amount of iron deposition could reflect the extent of tissue damage; thus, iron could be used as a biomarker to predict clinical outcome. This is a reasonable hypothesis given recent findings (27), which show very clear iron deposition encircling dilated veins in MS. The source of this iron is still unclear, but it could result from microhemorrhaging and hemosiderin buildup (27). Additionally, our results appear to indicate that chronic lesions may vanish on T2WI in some instances. If this is the case, then it may explain why the number of lesions on T2WI has not been very specific to the severity of the disease.

Apart from signal-to-noise, one of the key points about phase contrast is that it is independent of field strength if the product of field strength and TE is kept constant. Therefore, for the first time, it is possible to make comparisons of studies across systems and across field strengths and reasonably expect to get the same images (42). This should make SWI globally applicable in clinical trials on all manufacturers' systems.

In conclusion, we have shown that SWI has the potential to recognize the presence of iron in MS lesions, visualize lesions missed by conventional methods and visualize different lesion characteristics. The iron may be from blood or other iron sources sequestered by macrophages in the form of hemosiderin. Future studies should focus on monitoring iron levels along with cognitive and motor evaluations of the patient as a possible means to have a more specific imaging test of the patient's clinical status.

ACKNOWLEDGMENTS

The authors thank Alexander S. Boikov and Charbel A. Habib for their assistance in editing and revising this work. We also thank Siemens Medical Solutions for their continued support of our research.

REFERENCES

1. Noseworthy JH, Wolinsky JS, Lublin FD, et al. Linomide in relapsing and secondary progressive MS, part I: trial design and clinical results. North American Linomide Investigators. Neurology 2000; 54:1726–1733.
2. Weinshenker BG, Rice GP, Noseworthy JH, et al. The natural history of multiple sclerosis: a geographically based study. 3. Multivariate analysis of predictive factors and models of outcome. Brain 1991;114:1045–1056.
3. Keegan BM, Noseworthy JH. Multiple sclerosis. Annu Rev Med 2002;53:285–302.
4. Evangelou N, Esiri MM, Smith S, Palace J, Matthews PM. Quantitative pathological evidence for axonal loss in normal appearing white matter in multiple sclerosis. Ann Neurol 2000;47:391–395.
5. Hohlfeld R. Biotechnological agents for the immunotherapy of multiple sclerosis: principles, problems and perspectives. Brain 1997; 120:865–916.
6. Haacke EM, Wang Y, Yu Y, et al. Artery and vein separation using susceptibility-dependent phase in contrast-enhanced MRA. J Magn Reson Imaging 2000;12:661–670.
7. Tjoa CW, Benedict RH, Weinstock-Guttman B, Fabiano AJ, Bakshi R. MRI T2 hypointensity of the dentate nucleus is related to ambulatory impairment in multiple sclerosis. J Neurol Sci 2005;234:17–24.
8. MacKay A, Laule C, Vavasour I, Bjarnason T, Kolind S, Mädler B. Insights into brain microstructure from the T2 distribution. Magn Reson Imaging 2006;24:515–525.
9. Laule C, Leung E, Lis DK, et al. Myelin water imaging in multiple sclerosis: quantitative correlations with histopathology. Multiple Sclerosis 2006;12:747–753.
10. Jensen JH, Lu H, Inglese M. Microvessel density estimation in the human brain by means of dynamic contrast-enhanced echo-planar imaging. Magn Reson Med 2006;56:1145–1150.
11. Inglese M, van Waesberghe JH, Barkhof F, et al. The effect of interferon beta-1b on quantities derived from MT MRI in secondary progressive MS. Neurology 2003;60:853–860.

12. de Groot CJ, Bergers E, Kamphorst W, et al. Post-mortem MRI-guided sampling of multiple sclerosis brain lesions: increased yield of active demyelinating and (p)reactive lesions. Brain 2001;124: 1635–1645.
13. van Waesberghe JH, Kamphorst W, de Groot C, et al. Axonal loss in multiple sclerosis lesions: magnetic resonance imaging insights into substrates of disability. Ann Neurol 1999;46:747–754.
14. van Walderveen MA, Barkhof F, Hommes OR, et al. Correlating MRI and clinical disease activity in multiple sclerosis: relevance of hypointense lesions on short-TR/short-TE (T1-weighted) spin-echo images. Neurology 1995;45:1684–1690.
15. Morgen K, Jeffries NO, Stone R, et al. Ring enchancement in multiple sclerosis: marker of disease severity. Multiple Sclerosis 2001; 7:167–171.
16. Filippi M, Rocca MA, Rovaris M. Clinical trials and clinical practice in multiple sclerosis: conventional and emerging magnetic resonance imaging technologies. Curr Neurol Neurosci Rep 2002;2: 267–276.
17. Fu L, Matthews PM, de Stefano N, et al. Imaging axonal damage of normal-appearing white matter in multiple sclerosis. Brain 1998; 121:103–113.
18. Zivadinov R. Can imaging techniques measure neuroprotection and remyelination in multiple sclerosis? Neurology 2007;68:72–82.
19. Pike GB, de Stefano N, Narayanan S, et al. Combined magnetization transfer and proton spectroscopic imaging in the assessment of pathologic brain lesions in multiple sclerosis. AJNR Am J Neuroradiol 1999;20:829–837.
20. Schenck JF, Zimmerman EA. High-field magnetic resonance imaging of brain iron: birth of a biomarker? NMR Biomed 2004;17:433–445.
21. LeVine SM, Macklin WB. Iron-enriched oligodendrocytes: a reexamination of their spatial distribution. J Neurosci Res 1990;26: 508–512.
22. Dwork AJ, Schon EA, Herbert J. Nonidentical distribution of transferrin and ferric iron in human brain. Neuroscience 1988;27:333–345.
23. Francois C, Nguyen-Legros J, Percheron G. Topographical and cytological localization of iron in rat and monkey brains. Brain Res 1981;215:317–322.
24. Connor JR, Snyder BS, Arosio P. A quantitative analysis of isoferritins in select regions of aged, parkinsonian, and Alzheimer's diseased brains. J Neurochem 1995;65:717–724.
25. Levine SM, Chakrabarty A. The role of iron in the pathogenesis of experimental allergic encephalomyelitis and multiple sclerosis. Ann N Y Acad Sci 2004;1012:252–266.
26. Craelius W, Migdal MW, Luessenhop CP, et al. Iron deposits surrounding multiple sclerosis plaques. Arch Pathol Lab Med 1982; 106:397–399.
27. Zamboni P. The Big Idea: iron-dependent inflammation in venous disease and proposed parallels in multiple sclerosis. J R Soc Med 2006;99:589–593.
28. Tozer DJ, Davies GR, Altmann DR, Miller DH, Tofts PS. Correlation of apparent myelin measures obtained in multiple sclerosis patients and controls from magnetization transfer and multicompartmental T2 analysis. Magn Reson Med 2005;53:1415–1422.
29. Bakshi R, Ariyaratana S, Benedict RH, Jacobs L. Fluid attenuated inversion recovery magnetic resonance imaging detects cortical and juxtacortical multiple sclerosis lesions. Arch Neurol 2001;58: 742–748.
30. Drayer BP, Burger P, Hurwitz B, et al. Reduced signal intensity on MR images of the thalamus and putamen in multiple sclerosis: increased iron content? AJR Am J Roentgenol 1987;149: 357–363.
31. Ge Y, Jensen JH, Lu H, et al. Quantitative assessment of iron accumulation in the deep gray matter of multiple sclerosis by magnetic field correlation imaging. AJNR Am J Neuroradiol 2007;28: 1639–1644.
32. Haacke EM, Xu Y, Cheng YC, Reichenbach JR. Susceptibility weighted imaging. Magn Reson Med 2004;52:612–618.
33. Reichenbach JR, Venkatesan R, Yablonskiy DA, Thompson MR, Lai S, Haacke EM. Theory and application of static field inhomogeneity effects in gradient-echo imaging. J Magn Reson Imaging 1997;7: 266–279.
34. Haacke EM, Cheng NY, House MJ, et al. Imaging iron stores in the brain using magnetic resonance imaging. Magn Reson Imaging 2005;23:1–25.
35. Haacke EM, Ayaz M, Khan A, et al. Establishing a baseline phase behavior in magnetic resonance imaging to determine normal vs. abnormal iron content in the brain. J Magn Reson Imaging 2007; 26:256–264.
36. Duyn J, van Gelderen P, Li TQ, de Zwart J, Koretsky AP, Fukunaga M. High-field MRI of brain cortical substructure based on signal phase. Proc Natl Acad Sci USA 2007;104:11796–11801.
37. Haacke EM, Lai S, Yablonskiy DA, Lin W. In vivo validation of the BOLD mechanism: a review of signal changes in gradient echo functional MRI in the presence of flow. Intl J Imaging Sys Technol 1995;6:153–163.
38. McDonald WI, Compston A, Edan G, et al. Recommended diagnostic criteria for multiple sclerosis: guidelines from the international panel on the diagnosis of multiple sclerosis. Ann Neurol 2001;50: 121–127.
39. Bielekova B, Martin R. Development of biomarkers in multiple sclerosis. Brain 2004:127;1463–1478.
40. Prineas JW, Kwon EE, Cho ES, et al. Immunopathology of secondary-progressive multiple sclerosis. Ann Neurol 2001;50:646–657.
41. Lublin FD, Reingold SC. Defining the clinical course of multiple sclerosis: results of an international survey. National Multiple Sclerosis Society (USA) Advisory Committee on Clinical Trials of New Agents in Multiple Sclerosis. Neurology 1996;46:907–911.
42. Rauscher A, Sedlacik J, Barth M, Mentzel H-J, Reichenbach J.R. Magnetic susceptibility-weighted MR phase imaging of the human brain. AJNR 2005;26:736–742.